Karlsruher Institut für Technologie

FAKULTÄT FÜR PHYSIK

PHYSIKALISCHES PRAKTIKUM FÜR FORTGESCHRITTENE

PRAKTIKUM MODERNE PHYSIK

Gruppe Nr. _____ Kurs: **Mo1** **Mo2** **Mi3**

zutreffendes bitte ankreuzen

aktuelles Semester angeben

Versuch: _____

Namen: _____

_____

Assistent: _____

durchgeführt am: _____

Protokollabgabe am: _____

_____

vom Betreuer auszufüllen

Note gesamt [+] [0] [-]

Anerkannt: _____

(Datum Unterschrift)

Datum Rückgabe: _____

Bemerkung:

Contents

List of Figures

1. Introduction

The investigation of semiconductor materials, due to their significant applications in various technological fields, is a cornerstone of condensed matter physics. This experiment is conducted to analyze the optical properties of different semiconductor materials, employing spectroscopic techniques to elucidate their fundamental characteristics. Essential concepts such as transmission and absorption coefficients, Fabry-Perot interferences, and the band structure of semiconductors are explored. Furthermore, the study encompasses the analysis of the density of states in both three-dimensional and two-dimensional systems, with a focus on phenomena like excitons, quantum wells, and quantum dots.

A diverse set of samples has been selected for this experiment, each offering distinct perspectives on the optical behavior of semiconductor materials. These include a glass rod embedded with $CdS/CdSe$ colloids, a thin Cu_2O crystal, a $GaAs/Al_{0.3}Ga_{0.7}$ As Multiple Quantum Well (MQW), a CdS crystal, and a thick Cu_2O crystal. These samples provide an investigative platform for examining the effects of quantum confinement and material composition on optical properties.

The experimental approach is designed to conduct a comprehensive spectroscopic analysis. The transmission spectra of the colloidal rod are measured at various positions to detect shifts in absorption edges. The influence of light polarization on the transmission properties of the CdS crystal is also examined. In addition, the effects of cryogenic temperatures on the transmission spectrum of the MQW sample are observed, emphasizing the temperature dependence of semiconductor properties. Comparative analysis of the absorption spectra of Cu_2O crystals with differing thicknesses is conducted, shedding light on the impact of physical dimensions in optical absorption.

This report aims to integrate the experimental observations with theoretical aspects of semiconductor spectroscopy, providing an in-depth understanding of the optical phenomena exhibited by these materials.

1.1 Transmission and Absorption Coefficients

The interaction of light with a solid body encompasses transmission, reflection, and absorption, which can be quantitatively described by respective coefficients. These coefficients are fundamental in characterizing the optical behavior of materials:

$$T = \frac{I_T}{I_0} \tag{1.1}$$

$$A = \frac{I_A}{I_0} \tag{1.2}$$

$$R = \frac{I_R}{I_0} \tag{1.3}$$

Here, T represents the transmission coefficient, A the absorption coefficient, and R the reflection coefficient. I_T, I_A, and I_R denote the intensities of the transmitted, absorbed, and reflected light, respectively, with I_0 being the intensity of the incident light. The sum of these coefficients equals unity due to the conservation of energy:

$$1 = R + T + A \tag{1.4}$$

For the absorption of light within the material, the Lambert-Beer law is applied, which defines the intensity of light at a depth x as:

$$I(x) = I_0 e^{-\mu x} \tag{1.5}$$

with μ representing the attenuation coefficient. This law is particularly relevant in determining the penetration depth of light in various semiconductor materials and the efficiency of light absorption depending on the material's properties.

Furthermore, in the context of semiconductors, absorption is a critical process where light with energy corresponding to or greater than the band gap can be absorbed, leading to electronic transitions from the valence to the conduction band. This absorption process can create sharp increases, or edges, in the absorption spectrum, which are indicative of the material's electronic band structure and band gap energy.

1.2 Fabry-Perot-Interferometer

A Fabry-Perot interferometer consists of two parallel mirrors separated by a distance d. The incoming light is reflected multiple times between the mirrors and interferes with itself. For constructive interference, the condition is given by:

$$\nu_m = \frac{c}{2d} \cdot m \quad (m \in \mathbb{N}) \tag{1.6}$$

where ν_m represents the frequency of the m-th order maximum, c is the speed of light, and m is an integer representing the order of the interference maximum. For the eigenmodes of the interferometer, and the free spectral range (FSR) which is the distance between two consecutive eigenmodes in the spectral domain, the following relation holds:

$$FSR = \nu_m - \nu_{m-1} = \frac{c_0}{2nd} \tag{1.7}$$

$$FSR = \frac{c_0}{2nd} \tag{1.8}$$

where c_0 is the speed of light in vacuum, and n is the refractive index of the medium between the mirrors.

The interferometer can be utilized to determine the thickness of solid layers by employing the relationship for constructive interference:

$$2nd = \left(m + \frac{1}{2}\right) \lambda \tag{1.9}$$

$$\Rightarrow l = 4d \cdot \frac{n}{\lambda} - 2m \tag{1.10}$$

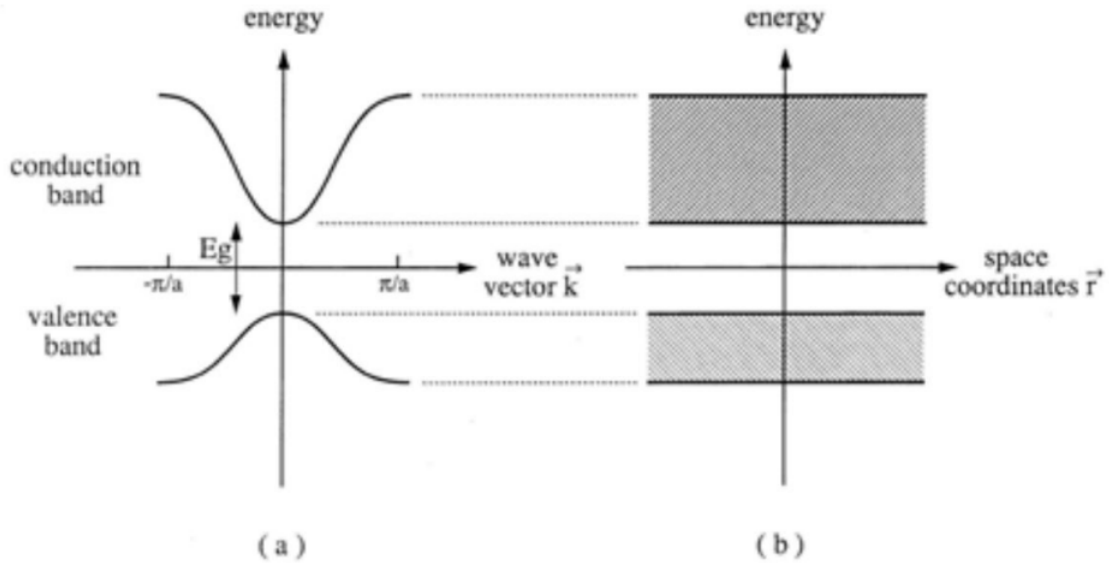

Figure 1.1: Energy band structure of a semiconductor showing the valence and conduction bands.

where l represents the physical thickness of the layer, and λ is the wavelength of light. By resolving for l, the thickness d can be determined through a linear fit of the data, making the Fabry-Perot interferometer an essential tool in the characterization of thin films in semiconductor devices.

1.3 Band Structure of Semiconductors

The band structure of semiconductors is a representation of the allowed and forbidden energy levels for electrons within a crystal lattice. It is derived from the periodic potential encountered by electrons, which leads to the formation of distinct energy bands:

$$k_z = \frac{n\pi}{a} \tag{1.11}$$

where k_z is the electron's wave vector along the z-axis, n is an integer, and a is the lattice constant. This relationship stems from the condition for standing waves in the lattice, and n represents the quantized energy levels within the band. The electron wave functions at the edges of the Brillouin zone are given by:

$$\nabla_k E(k) = 0 \tag{1.12}$$

A proper description of electron waves in solids requires considering the dispersion relation across the first Brillouin zone, reflecting the periodicity of the crystal lattice. The energy of free electrons in a periodic potential is described by:

$$E(k) = E_0 + \frac{\hbar^2 k^2}{2m^*} \tag{1.13}$$

where E_0 is the energy at the bottom of the conduction band, $\hbar$ is the reduced Planck constant, k is the wave vector, and m^* is the effective mass of the electron.

At the boundary of the first Brillouin zone, the Schrödinger equation admits solutions in the form of $\sin(k_x)$ and $\cos(k_z)$, resulting in the energy bands (or bandlines), which are the

eigenvalues of the equation. This band model is often visualized in a diagram known as the E-k diagram, which plots the energy of the electron states as a function of their wave vector.

Figure 1.1 illustrates the energy band structure in both reciprocal space and real space, depicting the conduction and valence bands, the band gap, and the wave vector k.

In semiconductors, the valence band is fully occupied, and the conduction band is partially occupied or completely empty, depending on the presence of free charge carriers. The existence of a band gap between these two bands is what defines the material as a semiconductor. The band gap's size and the nature of the electronic band structure determine whether a material behaves as an insulator, a semiconductor, or a metal.

1.4 Density of States in Semiconductors

The density of states (DOS) function in semiconductors is fundamental for determining the number of electron states at a given energy level that are available to be occupied. It is a key concept for predicting carrier concentrations and the resulting electrical and thermal properties of the material.

In a three-dimensional bulk semiconductor, the DOS for electrons in the conduction band and holes in the valence band varies with energy E according to the relations:

$$g_c(E) = \frac{1}{2\pi^2}\left(\frac{2m_e^*}{\hbar^2}\right)^{3/2}\sqrt{E - E_c} \tag{1.14}$$

$$g_v(E) = \frac{1}{2\pi^2}\left(\frac{2m_h^*}{\hbar^2}\right)^{3/2}\sqrt{E_v - E} \tag{1.15}$$

where $g_c(E)$ and $g_v(E)$ are the DOS for the conduction and valence bands respectively, m_e^* and m_h^* are the effective masses of the electrons and holes, E_c and E_v are the edges of the conduction and valence bands, and $\hbar$ is the reduced Planck constant.

In two-dimensional systems, such as quantum wells, the DOS becomes a step function due to the quantization of energy levels, which is represented as:

$$g_{2D}(E) = \frac{m^*}{\pi\hbar^2}\Theta(E - E_n) \tag{1.16}$$

where $g_{2D}(E)$ is the two-dimensional DOS, m^* is the effective mass, E_n is the quantized energy level, and Θ is the Heaviside step function.

These DOS functions are essential for interpreting optical absorption and emission processes in semiconductors. In optical spectroscopy, the shape of the DOS function influences the absorption coefficient, particularly near the band edges, where critical transitions occur between the valence and conduction bands.

Figure 1.2 provides a visual representation of the DOS for both three-dimensional and two-dimensional systems, showcasing the difference in energy distribution for these two cases.

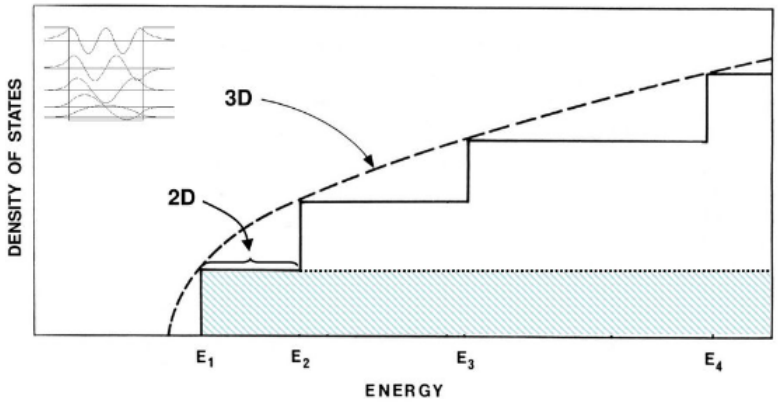

Figure 1.2: The density of states for three-dimensional and two-dimensional semiconductor systems..

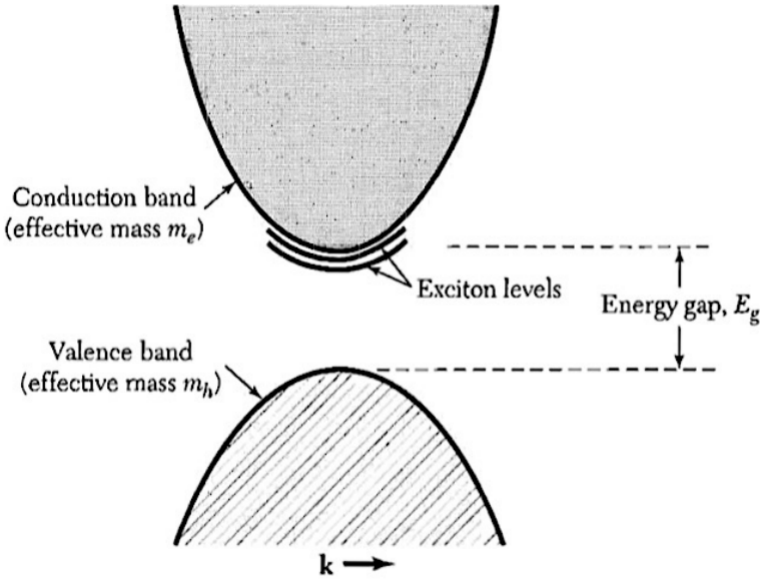

Figure 1.3: Schematic representation of exciton energy levels in a semiconductor.

1.5 Excitons in Semiconductors

Excitons are quasiparticles that arise in semiconductors when an electron is excited from the valence band to the conduction band, leaving behind a positively charged hole. The electron and hole, which are attracted to each other by Coulomb forces, can form a bound state, similar to a hydrogen atom, known as an exciton. The reduced mass μ of the exciton is given by $\mu = \frac{m_e m_h}{m_e + m_h}$, where m_e and m_h are the effective masses of the electron and hole, respectively. This system resembles the hydrogen atom and is characterized by discrete energy levels, known as exciton binding energies, given by:

$$E_b^X = R_y \frac{\mu}{m_0 \epsilon^2} \tag{1.17}$$

where E_b^X is the binding energy of the exciton, R_y is the Rydberg energy, μ is the reduced mass, m_0 is the free electron mass, and ϵ is the dielectric constant of the material.

The dispersion relation for excitons, which describes their energy as a function of the wave vector k, is expressed as:

$$E_X = E_g - \frac{E_b^X}{n_x^2} + \frac{\hbar^2 k^2}{2M} \tag{1.18}$$

where E_X is the energy of the exciton, E_g is the band gap of the semiconductor, n_x is the principal quantum number of the exciton, k is the total wave vector $k = k_e + k_h$, and M is the effective translational mass of the exciton ($M = m_e + m_h$).

These energy levels are typically located within the band gap, just below the conduction band, and can significantly influence the optical properties of the material due to the strong light-matter interaction associated with excitonic transitions.

Figure 1.3 depicts these exciton energy levels and illustrates how the binding energy of the exciton alters the energy landscape of the semiconductor, leading to distinctive features in optical spectra such as sharp absorption peaks.

1.6 Quantum Wells and Quantum Dots

Quantum wells and quantum dots are semiconductor structures that exhibit quantum confinement effects. In these nanostructures, the motion of charge carriers (electrons and holes) is confined to one or more dimensions, leading to quantized energy levels.

1.6.1 Quantum Wells

Quantum wells are created when a thin layer of semiconductor material is sandwiched between two barriers with a larger band gap. In these structures, charge carriers are confined in the direction perpendicular to the layer, resulting in a two-dimensional electron gas (2DEG) with energy levels given by:

$$E_n = \frac{\hbar^2 \pi^2 n^2}{2m^* L^2} + E_c \tag{1.19}$$

where E_n is the energy of the nth quantum level, $\hbar$ is the reduced Planck constant, m^* is the effective mass of the charge carrier, L is the width of the quantum well, E_c is the conduction band minimum, and n is an integer denoting the quantum number.

1.6.2 Quantum Dots

Quantum dots, on the other hand, are small semiconductor particles, typically ranging from 2 to 10 nanometers in diameter. In quantum dots, charge carriers are confined in all three spatial dimensions, which leads to a discrete set of energy levels similar to those of atoms, hence they are sometimes referred to as artificial atoms. The energy levels can be estimated by:

$$E_n = \frac{\hbar^2}{2m^*} \left(\frac{n_x^2}{L_x^2} + \frac{n_y^2}{L_y^2} + \frac{n_z^2}{L_z^2} \right) + E_c \tag{1.20}$$

where L_x, L_y, and L_z are the dimensions of the quantum dot, and n_x, n_y, and n_z are the quantum numbers associated with each spatial dimension.

Both quantum wells and quantum dots are utilized in various optoelectronic devices due to their size-tunable energy levels, which allow for the engineering of specific optical properties. They are widely used in applications such as lasers, light-emitting diodes (LEDs), and single-photon sources.

Figure 1.4 shows the energy level diagrams for a typical quantum well and a quantum dot, highlighting the quantized nature of the energy levels due to confinement.

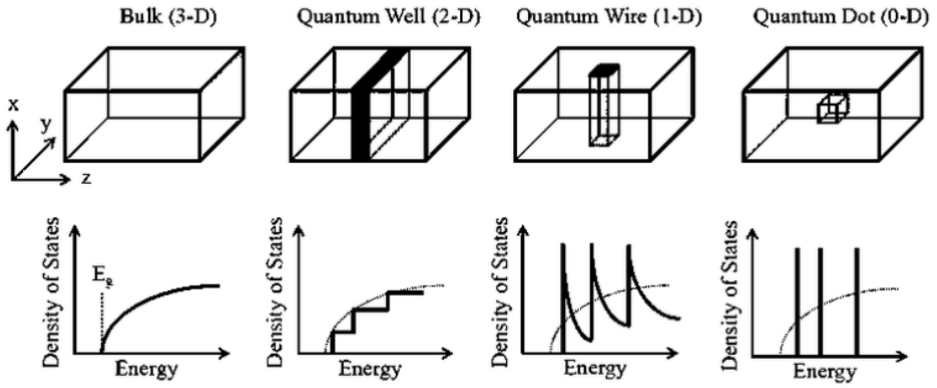

Figure 1.4: Energy level diagrams for a quantum well and a quantum dot.

In summary, the introduction has laid the groundwork for understanding the fundamental principles that govern the optical properties of semiconductor materials. The concepts of transmission and absorption coefficients, along with Fabry-Perot interferences, provide a basis for interpreting the interactions of light with semiconductor structures. The band structure and density of states in various dimensions have been discussed to illustrate the distribution of energy levels available to charge carriers in semiconductors. Excitons, as a result of electron-hole interactions, and the quantum mechanical phenomena observed in quantum wells and quantum dots have been introduced to explain the discrete energy levels that arise from quantum confinement effects.

The theoretical framework established in this introduction is crucial for the forthcoming experimental investigations. It will assist in elucidating the expected spectroscopic observations and in analyzing the data obtained from the experiments. The subsequent chapters will detail the experimental procedures, describe the methodology, and present the findings, which will then be comprehensively analyzed in the context of the theoretical background provided.

2. Experiment

This chapter outlines the experimental procedures employed to investigate the optical properties of various semiconductor samples. Each sample was selected to provide insight into different aspects of semiconductor physics, from the size-dependent quantum effects in colloidal systems to the impact of material thickness on optical absorption. Prior to the measurements, calibration of the photo detector was conducted under both bright and dark conditions to ensure accurate and reliable spectral data collection. This calibration is essential for compensating for any background noise and drift in the detector response, thus enabling a precise analysis of the transmission and absorption spectra.

2.1 Samples

A diverse array of semiconductor samples was systematically examined to assess their spectroscopic characteristics under varying conditions. The samples studied include:

- A glass rod embedded with $CdS/CdSe$ colloids with a gradient in particle size.
- Thin and thick crystals of Cu_2O.
- A $GaAs/Al_{0.3}Ga_{0.7}$ as Multiple Quantum Well structure.
- A CdS crystal.

The measurements performed on these samples were designed to reveal detailed information about the electronic transitions, band structure alterations, and effects of quantum confinement. The following sections will describe the specific methods used for each sample, the experimental setup, and the conditions under which each measurement was taken.

2.2 Measurement of Transmission Spectra of Sample 1

Sample 1 comprised a glass rod containing a gradient of CdS/CdSe colloids, with the particle size increasing along the length of the rod. This sample was chosen to investigate the size-dependent optical properties of the colloids, which are expected to exhibit quantum confinement effects that shift the absorption edge based on particle size.

The transmission spectra were measured using a spectrophotometer, which was carefully calibrated prior to the measurements. The sample was illuminated with a monochromatic light source ranging from 400 nm to 800 nm, covering the entire visible spectrum.

The rod was positioned within the spectrophotometer, and transmission spectra were collected at various points along its length. The intent was to identify positions where the colloidal particle size resulted in the most pronounced shifts in the absorption edges towards the blue (shorter wavelength) and red (longer wavelength) regions of the spectrum, respectively.

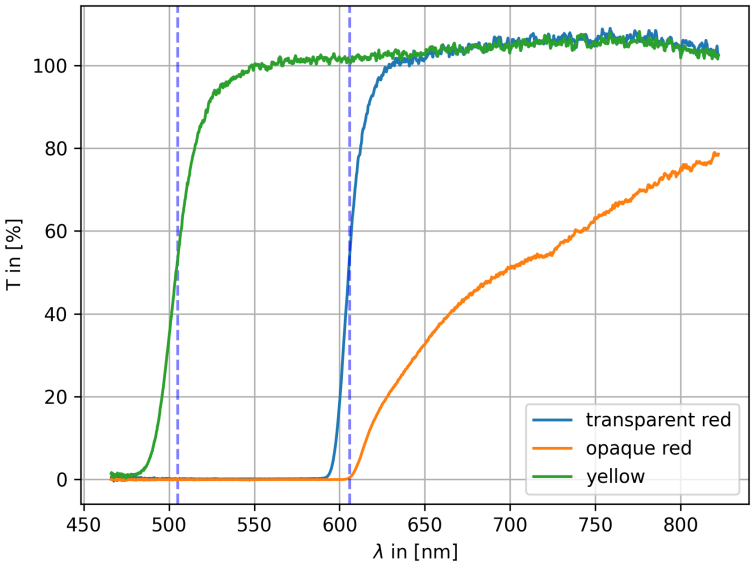

Figure 2.1: Transmission spectra of Sample 1, showing the variation in the absorption edge for colloids of different sizes. The spectra for 'transparent red', 'opaque red', and 'yellow' regions demonstrate the quantum size effect, with shifts in the onset of absorption corresponding to changes in colloid size.

To this end, the spectra were recorded at incrementally displaced positions along the rod, starting from the top where the colloid size was smallest, moving towards the bottom where the colloid size increased. This process was aided by the spectrophotometer's ability to scan across a range of wavelengths, thereby generating a detailed spectral profile at each measured point.

The measurement of the transmission spectra, illustrated in Figure 2.1 revealed distinct shifts in the absorption edges at different positions along the rod. These shifts are indicative of the changes in the band gap energy due to the varying sizes of the CdS/CdSe colloids, in accordance with the quantum size effect. The positions corresponding to the farthest blue and red shifts were marked for detailed analysis, as these extremes are critical for understanding the size-dependent optical behavior of the colloidal system.

2.3 Measurement of Transmission Spectra of Sample 2

Sample 2 consisted of a thin crystal of CdS, a material known for its strong interaction with light across the visible spectrum. This interaction is highly sensitive to the polarization of the incident light, making it an ideal candidate for studying polarization-dependent optical properties.

A spectrophotometer equipped with a rotatable polarizer was utilized to analyze the transmission spectra. The polarizer, positioned between the light source and the detector, allowed for precise control over the polarization state of the incident light. The CdS crystal was meticulously aligned within the setup to ensure that the polarized light traversed a region of the crystal characterized by uniform thickness and minimal surface imperfections.

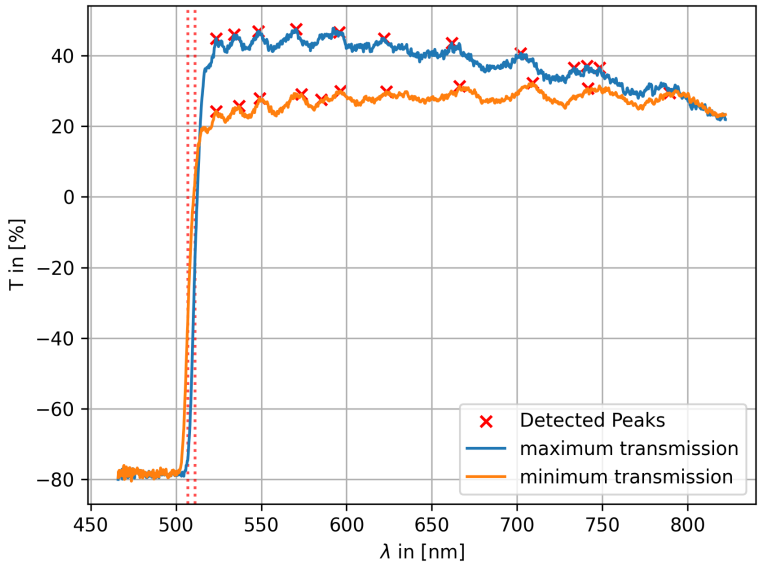

Figure 2.2: Polarization-dependent transmission spectra of the CdS crystal. The blue and red dotted lines indicate the positions of the absorption edge corresponding to the polarized light oriented to cause the blue and red shifts, respectively.

The measurement began with the identification of a sample position where the interference fringes were uniform, indicating a consistent optical path length across the light beam's cross-section. Once this position was established, the polarization of the incident light was adjusted to maximize the blue shift of the absorption edge. This setup captures the crystal's response to the E-vector orientation of the polarized light that emphasizes transitions associated with higher energy states.

Subsequently, a second measurement was taken with the polarization rotated by some degrees to induce a red shift in the absorption edge. This adjustment targets the opposite polarization state, revealing the energy levels associated with longer wavelengths.

The spectra obtained showed significant shifts in the absorption edge due to the change in light polarization. The blue shift corresponds to the energy absorption by the crystal's electronic structure at higher energies, while the red shift indicates lower energy transitions.

2.4 Transmission Spectrum Measurement of Sample 3 in Cryogenic Conditions

Sample 3 is a Multiple Quantum Well (MQW) structure composed of 60 layers of $GaAs/Al_{0.3}Ga_{0.7}$. MQWs are known for their sharp and well-defined electronic states that result from quantum confinement, which can be significantly affected by temperature changes.

The measurement setup included a cryostat capable of cooling the sample to the temperature of liquid nitrogen (77 K). Safety protocols were strictly followed, with the use of protective goggles and gloves while handling the cryogenic substance. The cryostat was equipped with optical access to allow for transmission spectroscopy within the specified wavelength range.

The MQW sample was cooled down by the cryostat, and the temperature was gradually lowered by the controlled introduction of liquid nitrogen. The transmission spectrum was continuously monitored in the spectral range from 600 nm to 820 nm. The measurement commenced as soon as the absorption lines stabilized, indicating that the sample had reached a steady-state temperature and the effects of thermal contraction had ceased.

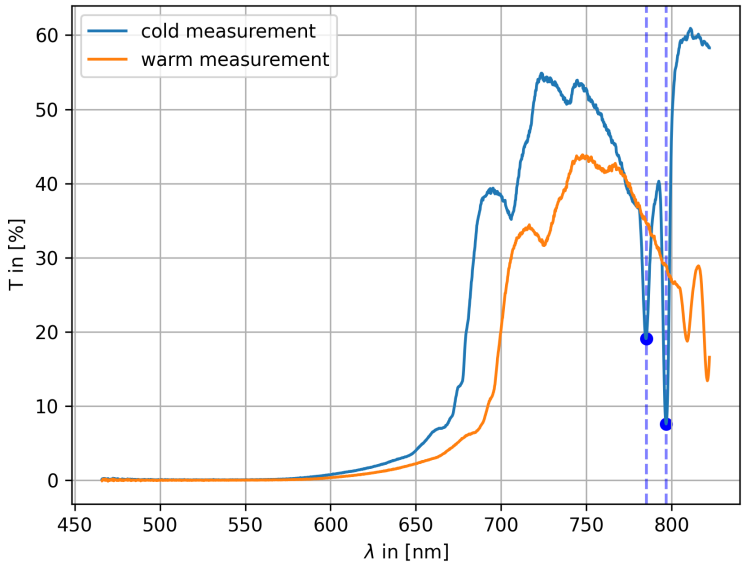

Figure 2.3: Transmission spectrum of the MQW structure at cryogenic temperatures, illustrating the temperature-induced shifts in the absorption lines.

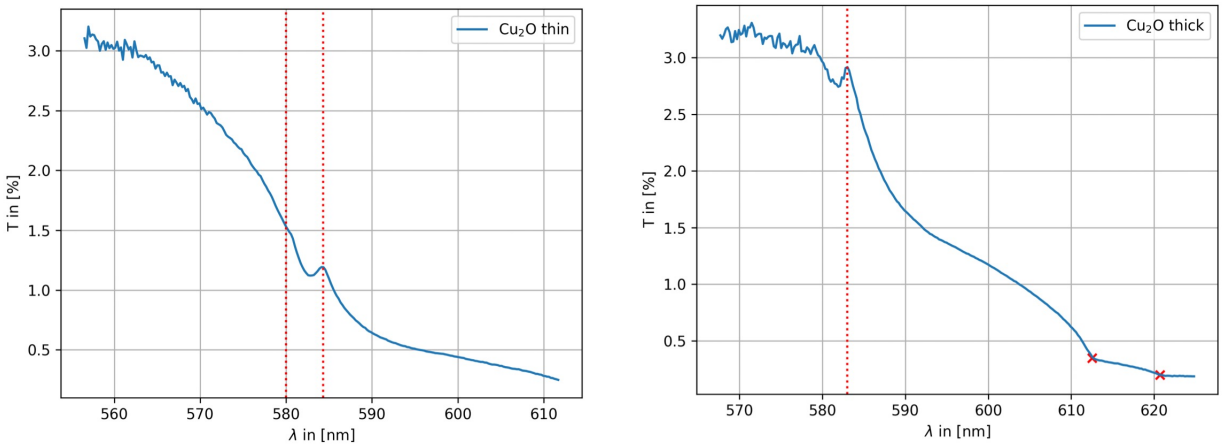

Figure 2.4: Comparison of absorption spectra for two Cu_2O crystals with different thicknesses (thin on the left, thick on the right), highlighting the influence of material thickness on the absorption properties.

Upon reaching cryogenic temperatures, notable shifts in the transmission spectrum were observed, with the absorption lines becoming more pronounced and shifting to higher energies, depicted in Figure 2.3. This behavior is indicative of the reduced thermal energy available to the charge carriers, leading to less broadening of the electronic states within the MQW.

2.5 Absorption Spectra Measurement of Cu_2O Crystals

Sample 2 and Sample 5 consisted of Cu_2O crystals, each with a distinct thickness. Cu_2O is a semiconductor with a direct band gap, and its optical properties are known to be influenced by the crystal thickness, which affects the interaction of light with the material.

The setup for measuring the absorption spectra included a spectrophotometer configured to capture a wide range of wavelengths. The Cu_2O crystals were individually mounted in the path of the light beam, ensuring that the entire beam passed through the crystal.

The absorption spectra for each Cu_2O crystal were measured over the same spectral range to directly compare the impact of thickness on the absorption characteristics. Care was taken to align each crystal so that the light beam was perpendicular to the surface, minimizing reflection losses and ensuring accurate absorption measurements.

The results for the two samples were expected to show variations in the absorption edge and overall absorption profile, illustrated in Figure 2.4. A thicker crystal typically exhibits more substantial absorption due to the increased path length of light within the material, leading to a higher probability of photon absorption.

In conclusion, the experimental chapter has documented the systematic approach taken to elucidate the optical properties of a variety of semiconductor samples through detailed spectroscopic analysis. The experiments conducted have not only showcased the size-dependent quantum effects in colloidal systems but also highlighted the impact of material properties, such as thickness and polarization, on the optical behavior of semiconductor crystals. The rigorous measurement protocols and the careful calibration of the equipment have ensured the collection of high-quality data, which is primed for in-depth analysis.

The insights gleaned from these experiments are invaluable for advancing the understanding of semiconductor physics and will serve as a firm foundation for the subsequent chapter, where a thorough analysis will be performed. The data analysis will aim to correlate the experimental findings with the theoretical framework established earlier, thereby providing a cohesive interpretation of the results obtained.

3. Evaluation/Data Analysis

3.1 Comparison of different light sources

Besides the conventional light bulb used in this experiment, which produces an approximately uniform light distribution over the observed wavelength spectrum, the spectrum of a LED light and a fluorescent light tube was recorded. These spectra can be seen in figure 3.3. Both spectra do not show a uniform distribution of emitted light and are therefore harder to normalize than the used conventional light bulb. As expected the light tube spectrum shows maxima at certain wavelengths corresponding to the emitting gas components in the light tube. In case of the LED the color coating alters the discrete emitted light, such that two maxima can be seen.

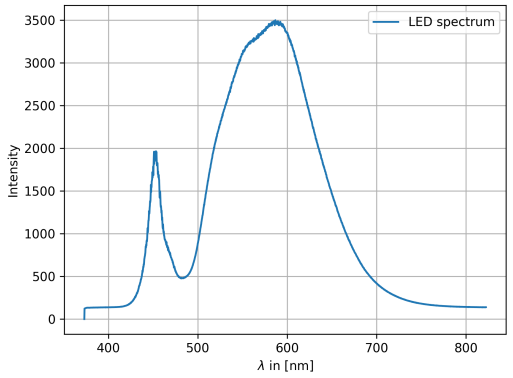

Figure 3.1: LED spectrum.

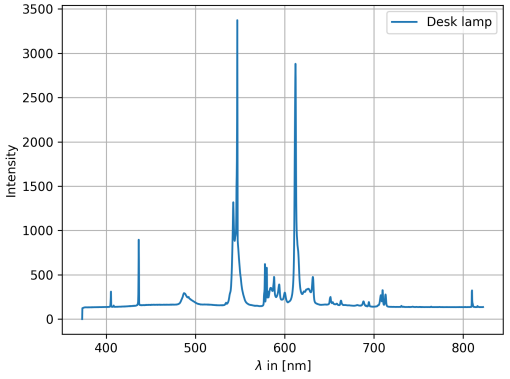

Figure 3.2: Fluorescent light tube spectrum.

Figure 3.3: Spectra of intensities for LED light and fluorescent light tube.

3.2 Determinating the radius of the smallest colloids in the sample

In calculation of the smallest colloids in the used CdS/CdSe sample is based on the assumption that the band-gap of this material approximately corresponds to the absorption edge of the largest colloids. The transmission spectrum was recorded for three different regions of the sample, the yellowish, transparent red and opaque red regions. Before each measurement, bright and dark measurements have been conducted to normalize the spectra and consider internal noise as well as external background. The obtained spectra are shown in figure 3.4. It follows that the absorption edge of the yellow area is blue shifted and the one of the transparent red are red shifted, in the following the first is referred to with indexes 'blue' and the latter as indexes 'red'. The minimal radius for colloids can be calculated through the relation to the energies corresponding to the absorption edges

$$E_{\text{blue}} = E_{\text{red}} + \frac{\hbar^2\pi^2}{2\mu R^2} \tag{3.1}$$

$$\rightarrow R_{\text{min}} = \sqrt{\frac{\hbar^2\pi^2}{2\mu(E_{\text{blue}} - E_{\text{red}})}}, \tag{3.2}$$

where μ is the reduced electron mass.

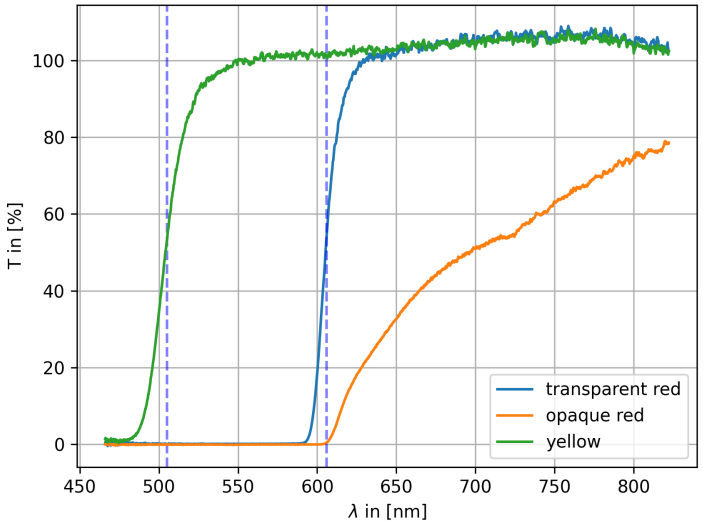

Figure 3.4: Transmission spectra of three recorded data sets. As expected the opaque red represents a very low transmission rate, the absorption edges of yellow and transparent red are approximated around $\lambda_{\text{blue}} = 505 \pm 10\,\text{nm}$ and $\lambda_{\text{red}} = 606 \pm 10\,\text{nm}$.

The approximation of the absorption edges yields

$$\lambda_{\text{blue}} = 505 \pm 10\,\text{nm}, \tag{3.3}$$
$$\lambda_{\text{red}} = 606 \pm 10\,\text{nm}. \tag{3.4}$$

Where the estimated error covers the whole measured absorption edge. The corresponding energies can be calculated through

$$E = \frac{hc}{\lambda}, \tag{3.5}$$

such that the minimal radius follows via 3.1

$$R_{\text{min}} = 2.14 \pm 0.1\,\text{nm}. \tag{3.6}$$

The error on R_{min} is obtained through error propagation.

3.3 Determining the layer thickness of the CdS sample

For this measurement a polarizer has been implemented between the CdS sample and the detector. After determining at which angle of the polarizer the transmission spectrum reaches a maxima and a minima, both spectra have been measured. In advance a bright and dark measurement have been conducted without the polarizer to normalize the spectra and consider internal noise as well as external background. The recorded spectra can be seen in figure 3.5. The band gap energies according to $\lambda_{\text{max}} = 511 \pm 5\,\text{nm}$ and $\lambda_{\text{min}} = 507 \pm 5\,\text{nm}$ can be calculated through 3.5 such that

$$E_{\text{max}} = 2.42 \pm 0.02\,\text{eV} \tag{3.7}$$
$$E_{\text{min}} = 2.44 \pm 0.02\,\text{eV}. \tag{3.8}$$

With errors resulting from error propagation.

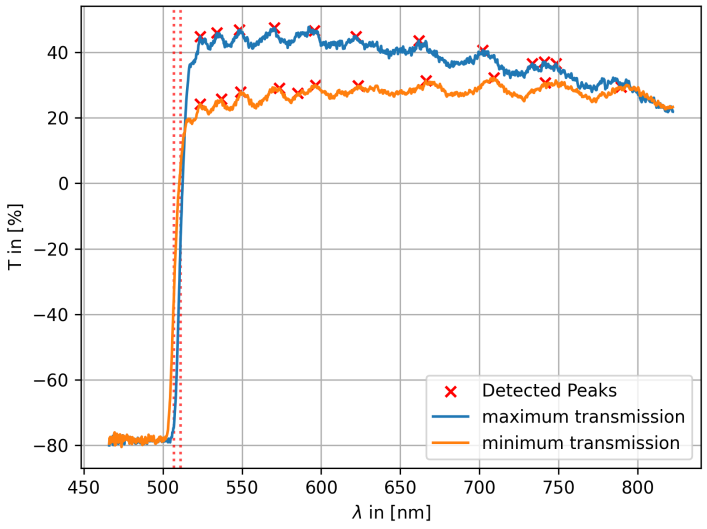

Figure 3.5: Transmission spectra of maximum and minimum transmission rate regarding the angle of the polarizer. The absorption edges are estimated to be located at $\lambda_{\text{max}} = 511 \pm 5\,\text{nm}$ and $\lambda_{\text{min}} = 507 \pm 5\,\text{nm}$. For further analysis the peaks in the transmission spectrum have been spotted with scipys peakfinder.

By using the Fabry-Perot-Method for extrema of the transmission spectra the layer thickness of the CdS sample can be obtained through relation 1.10. In this sense, the peaks of the transmission spectrum have been plotted with respect to their order corresponding to factors of $\frac{4n(\lambda)}{\lambda}$, such that the thickness can be obtained through a linear fit. The graph for the maximum transmission spectrum can be seen in figure 3.6, the one for the minimum transmission spectrum in figure 3.7. The resulting values for the layer thickness are

$$d_{\text{max}} = 1345 \pm 3 \pm 28\,\text{nm}, \tag{3.9}$$

$$d_{\text{min}} = 1566 \pm 3 \pm 38\,\text{nm}. \tag{3.10}$$

The systematical error is obtained through error propagation whilst the statistical error emerges from the linear regression.

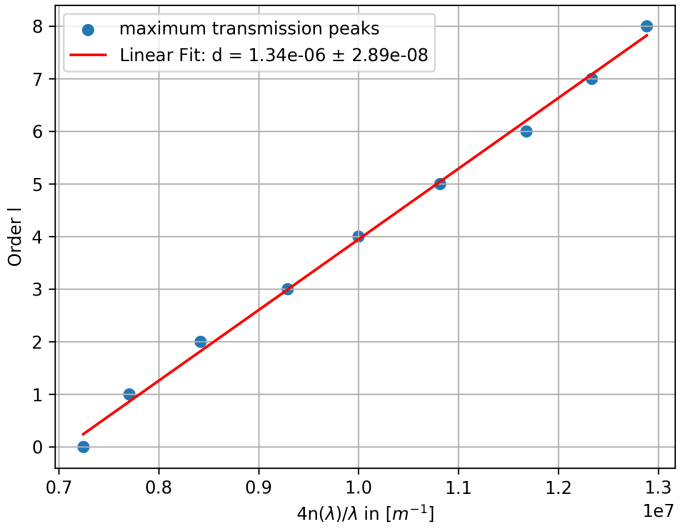

Figure 3.6: Linear regression for peaks of maximum transmission spectrum. The fit yields $\text{d}_{\text{max}} = 1.34 \cdot 10^{-6} \pm 2.89 \cdot 10^{-8}\,\text{m}$.

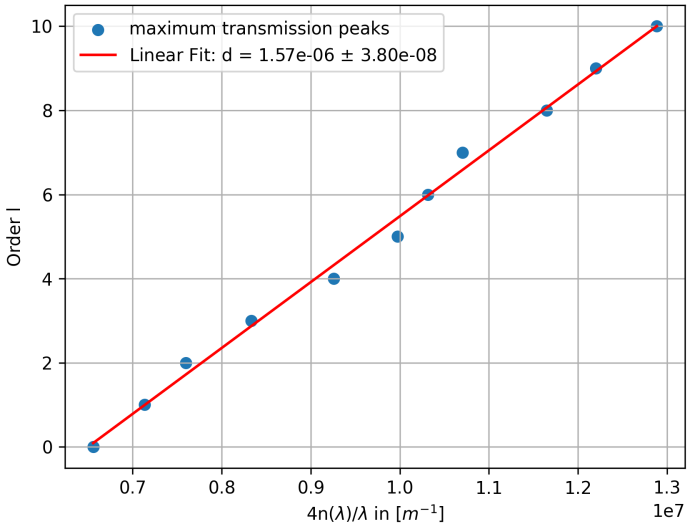

Figure 3.7: Linear regression for peaks of minimum transmission spectrum. The fit yields $\text{d}_{\text{min}} = 1.57 \cdot 10^{-6} \pm 3.8 \cdot 10^{-8}\,\text{m}$.

3.4 Determining the thickness of the GaAs quantum wells

The GaAs samples' transmission spectrum was recorded at room temperature and 77 K, the latter temperature was achieved by cooling the sample with liquid nitrogen. The spectra and the temperature-induced shifts in the absorption lines can be seen in figure 3.8. The minima detected with the Peakfinder option of scipy are found to be

$$\lambda_{\mathrm{hh}} = 797 \pm 1\,\mathrm{nm}, \tag{3.11}$$
$$\lambda_{\mathrm{lh}} = 785 \pm 1\,\mathrm{nm}. \tag{3.12}$$

From equation 1.18 the formulation for the thickness of the quantum well can be deduced to

$$l_z = \sqrt{\frac{\hbar^2\pi^2}{2}\left(\frac{m_{hh}}{M_{lh}} - \frac{m_{lh}}{M_{hh}}\right)\frac{1}{m_{lh}(E_g - E_{hh}) - m_{hh}(E_g - E_{lh})}}, \tag{3.13}$$

with the reduced masses m_{lh} and m_{hh}, the resulting mass $M_{xh} = m_e \cdot m_{xh}$ and the binding energies resulting from λ_{xh}, such that

$$l_z = 6.1 \pm 0.2\,\mathrm{nm}. \tag{3.14}$$

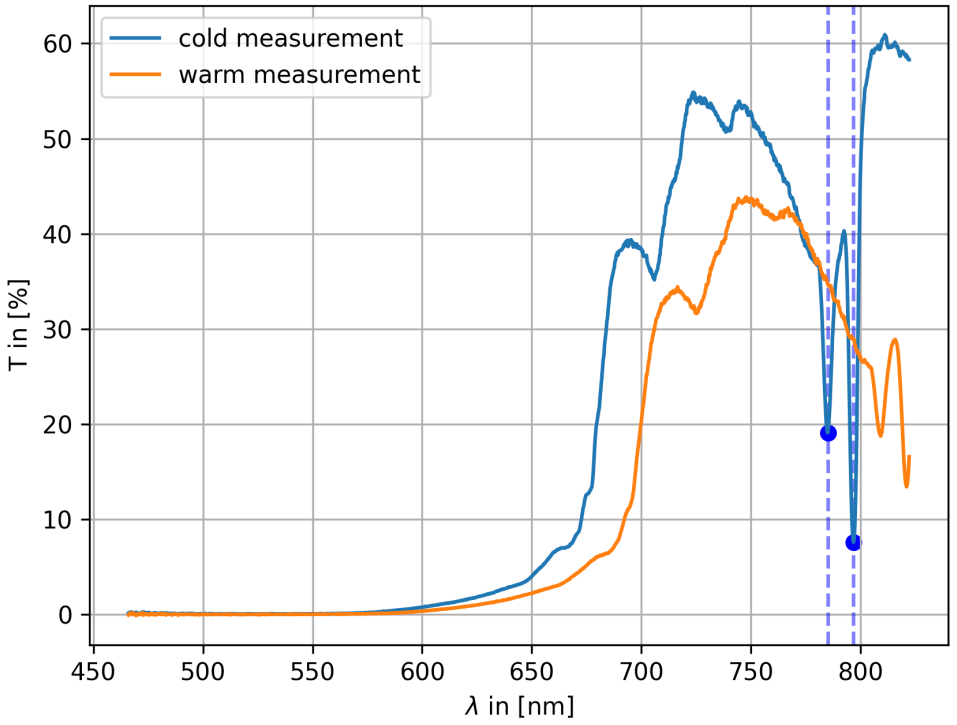

Figure 3.8: Transmission spectra at room temperature (warm measurement) and 77 K (cold measurement), as well as recorded minima for the cold measurement located at $\lambda_{\mathrm{hh}} = 797\,\mathrm{nm}$ and $\lambda_{\mathrm{lh}} = 785\,\mathrm{nm}$.

3.5 Identifying the np-exciton series in the Cu20 sample

In order to identify the np-exciton series in the Cu20 sample, the absorbance spectrum for a thick and thin sample have been recorded at 77 K. The spectrum for the thick sample can be seen in figure 3.9 and the one for the thin sample in figure 3.10

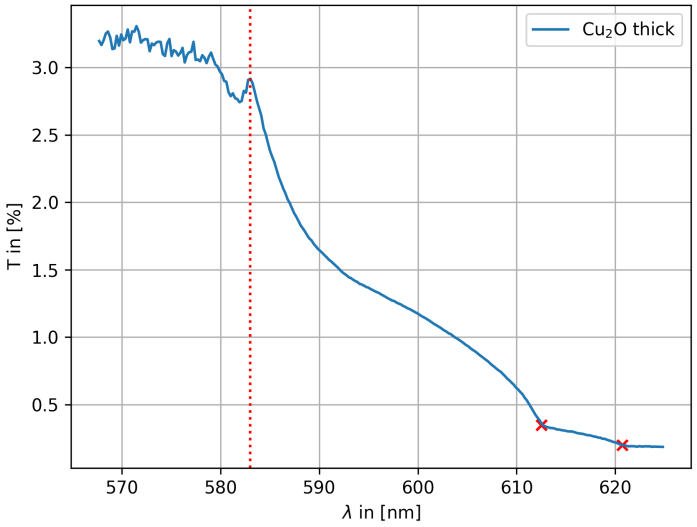

Figure 3.9: Absorbance spectrum of the thick Cu2O sample, the location of the 2p-exciton is marked by the red dotted line, the 1s-exciton is assumed to be located within the red crosses.

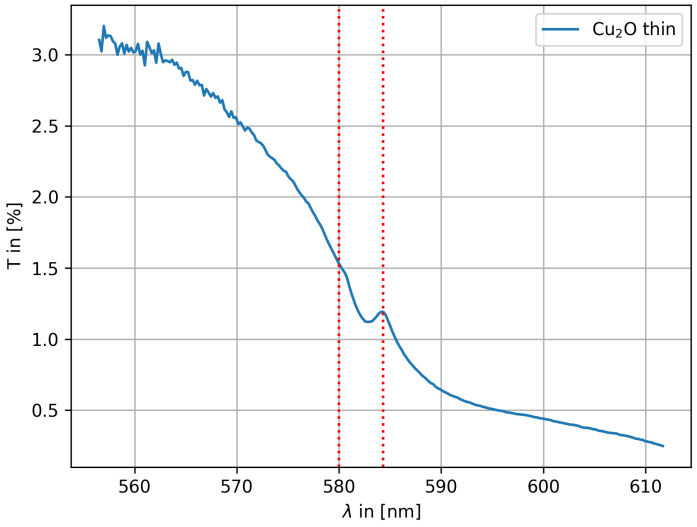

Figure 3.10: Absorbance spectrum of the thin Cu2O sample, the red dotted lines indicate the location of the 3p-exciton (left) and the 2p-exciton (right).

The locations are

$$\lambda_{\text{thick1}} = 583 \pm 1\,\text{nm}, \tag{3.15}$$
$$\lambda_{\text{thick2}} = 617 \pm 1\,\text{nm}, \tag{3.16}$$
$$\lambda_{\text{thin1}} = 580 \pm 1\,\text{nm}, \tag{3.17}$$
$$\lambda_{\text{thin2}} = 584 \pm 1\,\text{nm}. \tag{3.18}$$
$$\tag{3.19}$$

The band gap energy

$$E_g = \frac{n_2^2 E_{X,2} - n_1^2 E_{X,1}}{n_2^2 - n_1^2}, \tag{3.20}$$

and the binding energy

$$E_X^b = \frac{n_1^2 n_2^2 (E_{X,2} - E_{X,1})}{n_2^2 - n_1^2}, \tag{3.21}$$

can be calculated by using the quantum numbers $n_1 = 1$, $n_2 = 2$ for the thick sample and $n_1 = 2$ and $n_2 = 3$ for the thin sample. This results in

$$E_{\text{g,thick}} = 1.97 \pm 0.005\,\text{eV}, \tag{3.22}$$
$$E_{\text{g,thin}} = 2.111 \pm 0.007\,\text{eV}, \tag{3.23}$$
$$E^b_{\text{X,thick}} = 0.156 \pm 0.007\,\text{eV}, \tag{3.24}$$
$$E^b_{\text{X,thin}} = 0.105 \pm 0.04\,\text{eV}. \tag{3.25}$$

Bibliography

[1] given Literature